

ColorMapGAN: Unsupervised Domain Adaptation for Semantic Segmentation Using Color Mapping Generative Adversarial Networks

Onur Tasar, *Student member, IEEE*, S L Happy, *Member, IEEE*, Yuliya Tarabalka, *Senior member, IEEE*, Pierre Alliez

Abstract—Due to the various reasons such as atmospheric effects and differences in acquisition, it is often the case that there exists a large difference between spectral bands of satellite images collected from different geographic locations. The large shift between spectral distributions of training and test data causes the current state of the art supervised learning approaches to output poor maps. We present a novel end to end semantic segmentation framework that is robust to such shift. The key component of the proposed framework is Color Mapping Generative Adversarial Networks (ColorMapGAN), which can generate fake training images that are semantically exactly the same as training images, but whose spectral distribution is similar to the distribution of the test images. We then use the fake images and the ground-truth for the training images to fine-tune the already trained classifier. Contrary to the existing Generative Adversarial Networks (GAN), the generator in ColorMapGAN does not have any convolutional or pooling layers. It learns to transform the colors of the training data to the colors of the test data by performing only one element-wise matrix multiplication and one matrix addition operations. Thanks to the architecturally simple but powerful design of ColorMapGAN, the proposed framework outperforms the existing approaches with a large margin in terms of both accuracy and computational complexity.

Index Terms—Domain adaptation, semantic segmentation, dense labeling, convolutional neural networks, generative adversarial networks, GAN

I. INTRODUCTION

WITH the continuous proliferation and improvement of satellite sensors, numerous new generation satellite missions have been created, which has made it possible to collect huge amounts of data. The massive satellite data have introduced new challenges to the remote sensing community. *Semantic segmentation* or *dense labeling* is the task of assigning a thematic label to each pixel in the image. Without a doubt, among the challenges that the remote sensing community is facing today, dense labeling of the satellite images is one of the most important one, as a good solution for this problem is of paramount importance to generate and automatically update the maps.

Over the last few years, *convolutional neural networks* (CNNs) have become the most commonly used tool for the task of semantic segmentation. In particular U-net [1] and its

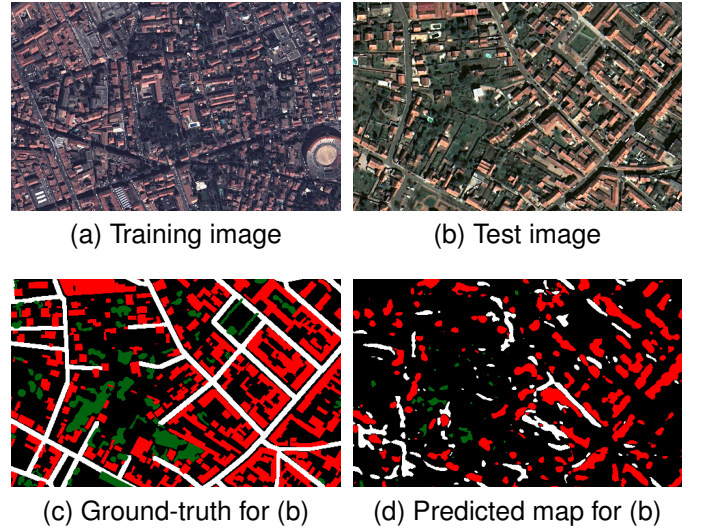


Fig. 1. An illustration for the domain adaptation problem, where we depict training and test images, the ground-truth for the test image, and the predicted map by U-net. In the ground-truth and in the predicted map, red, green, and white pixels correspond to building, tree, and road classes, respectively.

variants [2], [3] are receiving a growing attention due to their great success in different domains such as medical imaging and remote sensing. The main limitation of the aforementioned CNNs is their extreme sensitivity to the training data. Although they perform very well when both training and test data come from the same distribution [4], their performance severely decreases when there is a large difference between spectral bands of the training and the test images. Considering that nowadays new generation satellites with a short revisit time acquire huge amounts of images from different parts of the world, one cannot assume that the distribution of the images are always similar. In addition, depending on when and where the data are collected, a large intra-class variability might be encountered in remote sensing images. For instance, color distributions of the same objects may greatly differ in the images captured in different times of the day as a result of the illumination difference. Similarly, because of the atmospheric effects, in some cases, even the images collected by the same satellite sensors might have very different radiometry, which makes the segmentation task even harder. Fig. 1 illustrates such an example, where color distributions of the training and the test data collected by the same satellite are noticeably different.

O. Tasar, and P. Alliez are with Université Côte d’Azur and Inria, TITANE team, 06902 Sophia Antipolis, France. E-mail: onur.tasar@inria.fr

S L Happy is with Inria, STARS team, 06902 Sophia Antipolis, France.

Y. Tarabalka is with LuxCarta Technology, Parc d’Activité l’Argile, Lot 119b, Mouans Sartoux 06370, France

As shown in the figure, even a well trained U-net, which is considered as the state of the art in semantic segmentation of satellite images [5], generates a poor map.

The *unsupervised domain adaptation* assumes that annotations for any part of the test data are not available, and aims at generating high quality segmentations even when there is a large domain shift between the training and the test images. In such a setting, in order to increase generalization capabilities of the CNNs, one of the simplest and most common methods is to diversify the training data by applying various data augmentation techniques such as gamma correction and random contrast change [6]. However, even though these techniques help the CNNs to generalize slightly better, when spectral difference between the training and the test data is huge, the improvement is usually insufficient. Although a good solution for domain adaptation is indispensable for various applications, this problem has not been investigated intensively in the field of remote sensing. The limitations pointed out in this section have motivated us to design a methodology for this problem.

A. Related Work

The majority of the proposed approaches in the literature are based on the idea of *aligning distributions* of both training and test images in a common space using *generative adversarial networks (GAN)* so that the trained classifier could segment the test images well. FCNs in the Wild [7] reduces the global distribution difference between the training and the test images by minimizing an adversarial loss. Aligning the distributions of the extracted features from both the training and the test images is also a common approach [8], [9]. The distribution alignment could also be performed in multiple layers of the network instead of only the final output [10], [11]. Hong *et al.* add random noise to the training images [12]. They observe that perturbing the training images helps the GAN to adapt better to the test data. Saito *et al.* introduces a maximum classifier discrepancy based approach, which aligns the distributions by making use of class-specific decision boundaries [13]. The framework presented by Chen *et al.* utilizes Google Street View to collect unannotated images and to use their features. Curriculum Domain Adaptation (CDA) [14] performs the alignment both globally and on the generated super-pixels. Reality Oriented Adaptation (ROAD) [15] comprises two loss functions. The first one forces the weights of the trained model from the training images with the weights of the pre-trained model from ImageNet [16] to be as similar as possible. The second one handles the spatial aware domain adaptation by dividing the training and the test images into grids and minimizing distance between the grids of the training and the test images.

There have been attempts to solve the domain adaptation problem by *regularizing* or *normalizing specific layers* of the network, or by *self-learning*. The Fully Convolutional Tri-branch network (FCTN) [17] is one of the methods that falls into the category of self-learning. The presented network architecture consists of one encoder and three decoders. Two of the decoders pseudo-label the test image, the other one

learns from the pseudo-labels and the test image. A class-balanced self learning approach is proposed in CBST [18]. Introducing new normalization method, regularization technique, or new loss functions that are specific for domain adaptation problem is investigated in [19]–[22]. Romijnders *et al.* discuss the limitations of the traditional normalization methods such as batch normalization, and propose a new domain agnostic normalization layer that is more suitable for domain adaptation [19]. Saito *et al.* introduce a new adversarial dropout regularization technique [20]. The IBN-Net [21] combines the batch normalization with the instance normalization [23] to increase the generalization capability. Zhu *et al.* proposes a new conservative loss [22].

Another way to approach the unsupervised domain adaptation problem is to perform *image to image translation (I2I)* between a source and a target domain. The I2I approaches such as CycleGAN [24], UNIT [25], MUNIT [26], and DRIT [27] aim to generate fake source images, which are indistinguishable from the target images. If one can generate fake training images, which are style-wise consistent with the test images and semantically consistent with the original training images, the fake images could be used to train a model from scratch or to fine-tune the already trained model on the original data. The main drawback here is that usually the fake training images generated by the I2I approaches contain artificial objects which do not exist in the original images. Hence, annotations for the original training images and the generated fake training images do not match. As a result, the model learns wrong information. To overcome this limitation, CyCADA [28] segments the original and the fake training images using the classifier trained on the original training data, and minimizes cross entropy loss between the segmentations. However, if the domain shift between the training and the test data is large, the classifier trained from the original training images will segment the fake training image poorly. If the segmentation for the training images is very good, but the predicted map for the fake training images is extremely noisy we cannot expect adding such a loss to prevent artificial objects appearing. Another way to enrich the training data could be to perform neural style transfer, where content of an image and style of another image are combined [29]–[32]. However, they also cannot guarantee that the semantic structures will be preserved.

In the field of *remote sensing*, traditional domain adaptation approaches such as transfer component analysis (TCA) [33] have been investigated in a few works. For instance, the methodology presented by Matasci *et al.* [34] firstly extracts certain features from both the training and the test images and then aims to find transformation matrices to embed all the features in a common space using TCA. Finally, one can train a classifier using the embeddings for the training images and utilize embeddings for the test images to generate segmentations. However, this method requires feature engineering. Moreover, because of the matrix multiplications, performing large-scale segmentations may not be feasible. Qin *et al.* describes a super-pixel based approach [35]. However, it is usually not easy to generate perfect super-pixels, especially from satellite images.

B. Contributions

We study the problem of unsupervised domain adaptation for semantic segmentation, where training and test images are collected from completely different geographic locations, they have significant spectral distribution difference, and annotations for any part of the test images are not available. The way we approach the problem methodologically resembles to the image to image translation (I2I) approaches; we generate fake training images as if they came from the distribution of the test images. Instead of working on images acquired over separate geographic extents, if we had paired training and test images (e.g., images acquired from exactly the same geographic extent but in different day time), the problem would be easier, we could perform paired I2I [36].

The main challenge here is to generate fake training images that look like test images without destroying the semantic meaning in the original training images, even when the training and the test images are unpaired. If the semantic structures of the original training images are preserved in the fake training images, we can utilize the annotations for the original training images as well as the fake training images to fine-tune the already trained model from the original training data. When generating fake training images with the style of the test images, the I2I approaches presented in Sec. I-A fail to preserve the exact structures of the original training images, especially when we deal with satellite images containing a lot of complex and heterogeneous objects. Thus, the fake training images and the annotations do not match, which leads the model to learn incorrect information.

Contributions of this work are as follows:

1) *ColorMapGAN*: Our main contribution is novel ColorMapGAN which can generate fake training images that are semantically exactly the same as the original training images (i.e., location and shape of the objects such as roads, building, trees, etc. are exactly the same in the fake and in the original training images) and that are visually indistinguishable from the test images (i.e., the objects such as trees and buildings in the fake training images and the test images have similar spectral distributions). To do this, ColorMapGAN transforms the colors of the training images into the colors of the test images without doing any structural changes on the objects of the training images.

2) *Lower complexity*: Unlike the existing GANs in the literature, our generator does not perform any convolution or pooling operations. It transforms the colors of the training images with only one element-wise matrix multiplication and one matrix addition. Because our generator is architecturally substantially simpler compared to the existing GANs, the training time is significantly lower than the other approaches. In our experiments, we compare our approach with a methodologically similar and competitive method (CycleGAN [24]) in the computer vision community in terms of running times to train a model.

3) *Higher accuracy*: In our experiments, we perform city to city domain adaptation. We utilize the fake training images generated by our approach and by CycleGAN [24] to fine-tune the model trained from the original training images. In addition

to a methodologically similar approach (CycleGAN), we also compare our methodology with AdaptSegNet [10]. Despite its architecturally simple design, our framework enables to generate predicted maps with much higher accuracy than the others.

II. GENERATIVE ADVERSARIAL NEURAL NETWORKS

In machine learning, we can divide the models trained in a supervised setting into two groups: discriminative and generative models. In the field of image analysis, the discriminative models are usually trained to learn a mapping from a high dimensional input to class labels as in image categorization and segmentation problems. On the other hand, the generative models aim to estimate the distribution of the data samples so that new samples could be drawn from the estimation. Although the discriminative models have been commonly used in many application domains, the generative models have not been popular until recently. In 2014, Goodfellow *et al.* proposed the generative adversarial networks (GAN) [37], which is a novel approach to train a generative model.

GAN usually comprises a generative model G and a discriminative model D . The goal of G is to estimate the distribution of the real data and to output fake data from the estimation. G takes a random noise z as input, and represents a mapping to data space $G(z)$. We denote the distribution of the real data x by $p(x)$ and a prior on input noise variables by $p(z)$. Let us assume that the real data x and the fake data $G(z)$ are indicated by 1 and 0, respectively. D outputs a scalar between 0 and 1, and aims to maximize the probability of labeling x and $G(z)$ correctly. In other words, the goal of D is to discriminate between the real and the fake data. The objective function for D that is maximized during training is described as:

$$\max_D V(D) = \mathbb{E}_{x \sim p(x)} \log[D(x)] + \mathbb{E}_{z \sim p(z)} [\log(1 - D(G(z)))], \quad (1)$$

where \mathbb{E} is the expected value. G is simultaneously trained to minimize the objective function defined as:

$$\min_G V(G) = \mathbb{E}_{z \sim p(z)} [\log(1 - D(G(z)))]. \quad (2)$$

As a result, the minimax game played between G and D could be formulated as:

$$\min_G \max_D V(D, G) = \mathbb{E}_{x \sim p(x)} \log D(x) + \mathbb{E}_{z \sim p(z)} \log(1 - D(G(z))). \quad (3)$$

Once D and G are simultaneously trained for a sufficiently long time, D becomes good at discriminating the fake and the real data, and G becomes better at generating fake data that are indistinguishable from the real data.

Although GAN works well with shallow multi-layer perceptrons, they suffer from instability problems during training when a more complex network is used. Several approaches have been presented to address the instability issues. In DCGAN [38], instead of multilayer perceptrons, deep convolutional networks are used in both G and D , and certain architectural constraints are introduced for a more stable training. In WGAN [39], rather than the logarithms in Eq. (3),

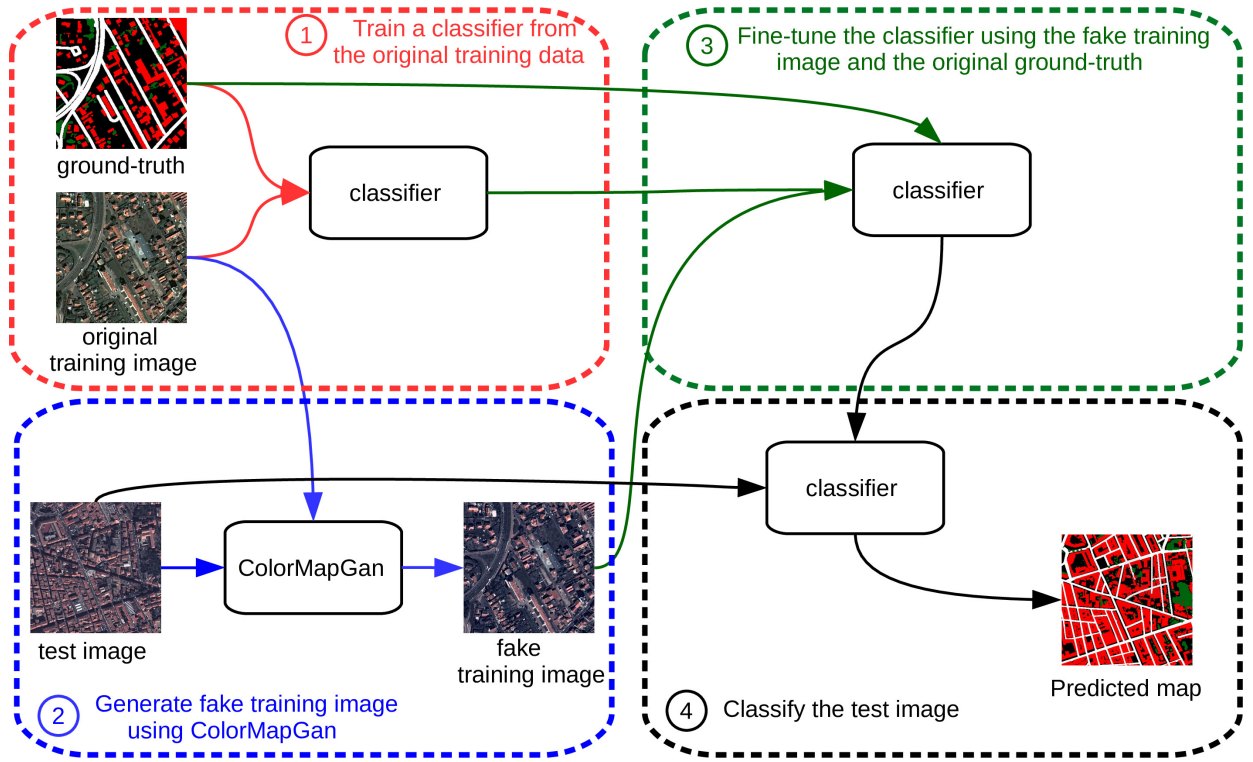


Fig. 2. The overall end to end framework.

Wasserstein distance is used to compute distance between the distributions, and gradient clipping is applied in the training stage. WGAN-GP [40] is an extension of WGAN, where a gradient penalty is performed to solve the limitations of the gradient clipping. LSGAN [41] proves that adopting the least squares loss function in Eq. (3) allows more stabilized training.

Finally, the original GAN was extended to conditional GAN in [42], where instead of generating the fake data from noise z , both G and D are conditioned on some extra information y . y can be class labels or data from other modalities. In this architecture, G learns a mapping from combination of z and y to the data space. If we consider y as the source data and x as the target data, G aims to learn a mapping from source domain to target domain. Inspired from this idea, conditional GANs have been used for several I2I works [24], [36].

III. METHODOLOGY

A. The Overall End to End Framework

Fig. 2 depicts the overall end to end framework which consists of 4 steps as follows:

- 1) *Training the initial classifier:* We train a Unet on the original training data.
- 2) *ColorMapGAN:* We generate fake training images that are semantically exactly the same as the original training images, but visually as similar as possible to the test images using the proposed ColorMapGAN.
- 3) *Fine-tuning:* We fine-tune the model obtained in step 1 using the fake training images and the ground-truth for the original training images.
- 4) *Classification:* Finally, we classify the test images.

We use a slightly modified version of U-net [1] as the classifier. We replace rectified linear activation units (ReLU) by leaky rectified linear activation units (Leaky-ReLU) for a better performance [43]. We also remove the batch normalization operation in each layer, since it uses the memory inefficiently. In the end to end framework, the steps 1, 3, and 4 are self-explanatory, whereas step 2 needs further explanation.

B. ColorMapGAN

1) *Generator:* The novelty of the proposed ColorMapGAN is in the architecturally simple but powerful design of its generator.

We denote a set of training image patches by $X = \{x_1, x_2, \dots, x_N\}$ and a set of test image patches by $Y = \{y_1, y_2, \dots, y_M\}$. $G(X)$ corresponds to the set of fake training patches generated by G . The goal of G is to generate $G(X)$ whose spectral distribution is as similar as possible to the distribution of Y , while keeping $G(X)$ and X semantically exactly the same. Contrary to the existing GANs in the literature, we do not use convolutional or pooling layers in G to preserve the exact semantics of X in $G(X)$.

Let us assume that X and Y are composed of 8 bit images comprising red, green, and blue channels. We denote by $R = \{0, 1, \dots, 255\}$, $G = \{0, 1, \dots, 255\}$, and $B = \{0, 1, \dots, 255\}$, the values each color band of the pixels can take. We denote all the possible 16,777,216 ($256 \times 256 \times 256$) colors by RGB , which is defined as:

$$RGB = R \times G \times B, \quad (4)$$

where \times stands for the Cartesian product. In order to transform RGB to another color matrix $R'G'B'$, we use a scale W

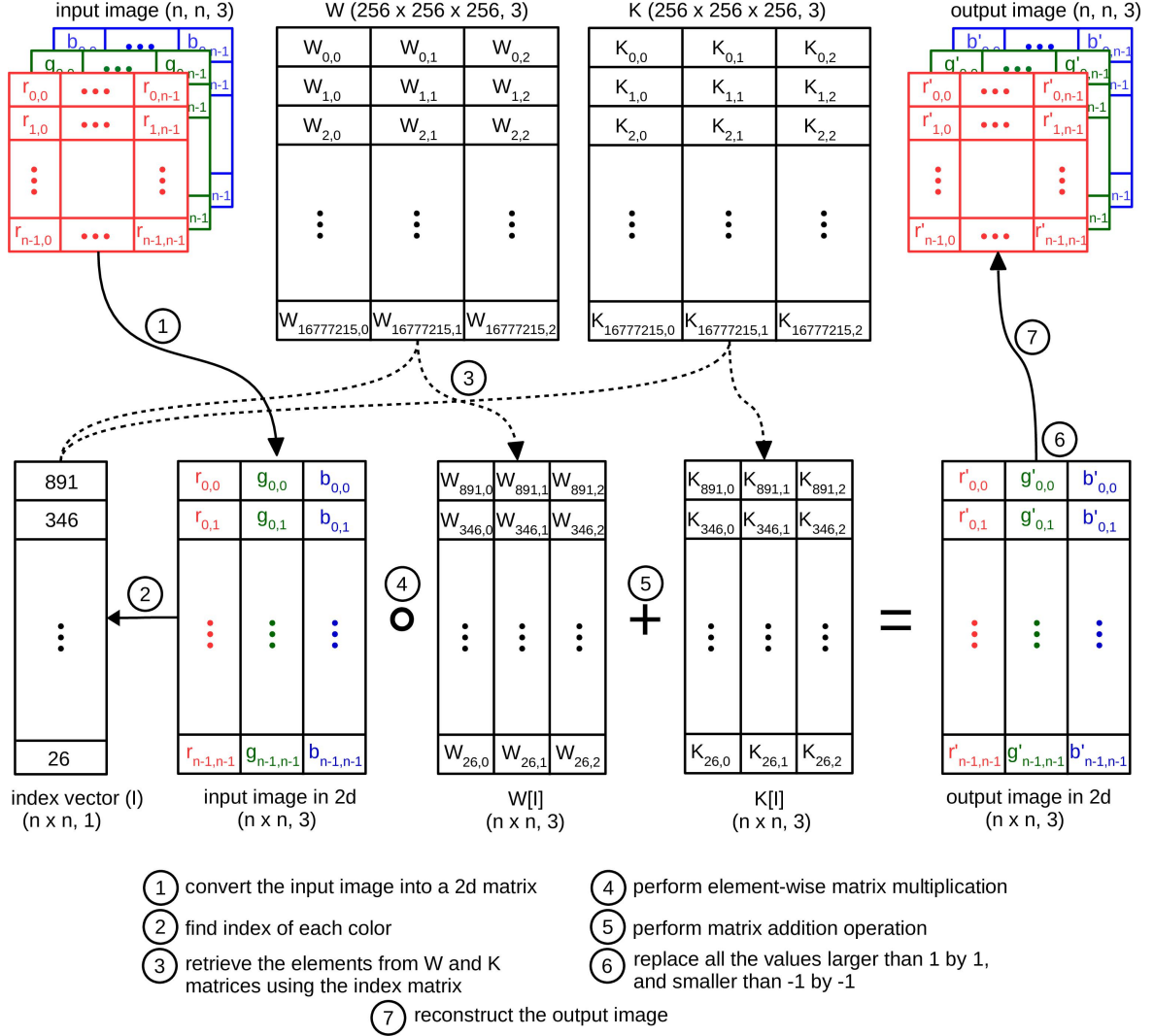


Fig. 3. The overall flowchart for the feedforward pass of the generator.

and a shift K matrices with the same size as RGB . $R'G'B'$ could be computed as:

$$R'G'B' = RGB \circ W + K, \quad (5)$$

where \circ is the element-wise product. The only learnable parameters of our G are W and K . Before the training starts, we initialize W with ones and K with zeros. Hence, at the end of the first iteration, the input and the output of G are exactly the same.

The main bottleneck for computing Eq. (5) is the computational complexity. Since each of RGB , W , and K matrices has more than 50 millions of elements ($256 \times 256 \times 256 \times 3$), it is not feasible to perform the operation defined in Eq. (5) on a GPU. However, the number of colors in a training image patch is much lower than the number of all the possible colors. Therefore, it is sufficient to update only the elements of W and K which transform the colors that are available in the training patch. To do this, we use an index vector I that is defined as:

$$I = r \times 256 \times 256 + g \times 256 + b, \quad (6)$$

where r , g , b are red, green, blue values of all the pixels in the training patch. After the elements of I are found, we normalize and center each $x_i \in X$ and $y_j \in Y$ by first dividing by 127.5 and then subtracting 1 so that each color channel ranges between -1 and 1 . We then partially update $R'G'B'$ as:

$$R'G'B'[I] = RGB[I] \circ W[I] + K[I], \quad (7)$$

where $[\cdot]$ operation corresponds to retrieving the rows of an arbitrary 2D matrix indexed by the given vector. Then, in $R'G'B'[I]$, we replace the elements that are bigger than 1 and smaller than -1 by 1 and -1, respectively. To range all the values in $R'G'B'[I]$ between 0 and 255, we then use the denormalization function DN that is defined as:

$$DN(p) = \lfloor (p + 1) \times 127.5 \rfloor, \quad (8)$$

where p is a 2D input matrix. The final output of G can be obtained by reshaping $DN(R'G'B'[I])$ back to the shape of the input patch. In each training iteration, we update only $W[I]$ and $K[I]$.

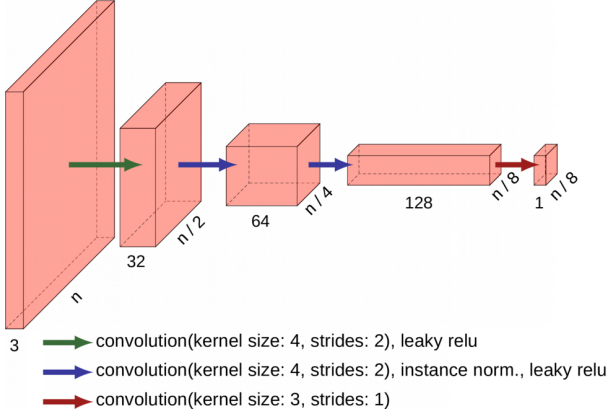


Fig. 4. The architecture of the discriminator. n corresponds to the patch size, and the number below each layer is the depth.

Fig. 3 illustrates the overall flowchart for the feedforward pass of G .

2) *Discriminator*: The discriminator in ColorMapGAN is architecturally the same as CycleGAN [24] (see Fig. 4). Instead of outputting a single scalar for the whole image patch to determine if the patch is real or fake, this discriminator generates a two dimensional matrix. Each element of the matrix is used to locally determine whether the input patch is real or fake. We then take average of all the elements of the matrix to yield a final value.

As we mention in Sec. II, GANs suffer from the instability issues; therefore, other objective functions have been proposed as an alternative to Eqs. 1, 2, and 3. We prefer to use the functions presented in LSGAN [41]. Thus, for D , the objective function that is minimized during training becomes:

$$\min_D V(D) = \mathbb{E}_{x \sim p(x)} [(D(x) - 1)^2] + \mathbb{E}_{y \sim p(y)} [(D(G(y)))^2]. \quad (9)$$

The objective function for G is defined as:

$$\min_G V(G) = \mathbb{E}_{y \sim p(y)} [(D(y) - 1)^2]. \quad (10)$$

We train D and G simultaneously by minimizing the Eqs. 9 and 10.

IV. EXPERIMENTS

A. Methods Used for Comparison

Unet [1]: Here, we simply train a Unet from the training images and segment the test images without performing any type of domain adaptation techniques.

CycleGAN [24]: Similar to ColorMapGAN, this is another unpaired I2I method. In this methodology, in addition to G , there is one more generator F . G is used to learn a mapping from training images to test images, whereas F learns a mapping from test images to training images. The methodology requires that the mapping from training images to test images and another consecutive mapping from test images to training images reproduce the original training images. This constraint is enforced by minimizing the L1 norm between $F(G(X))$ and X , and between $G(F(Y))$ and Y . For a fair comparison

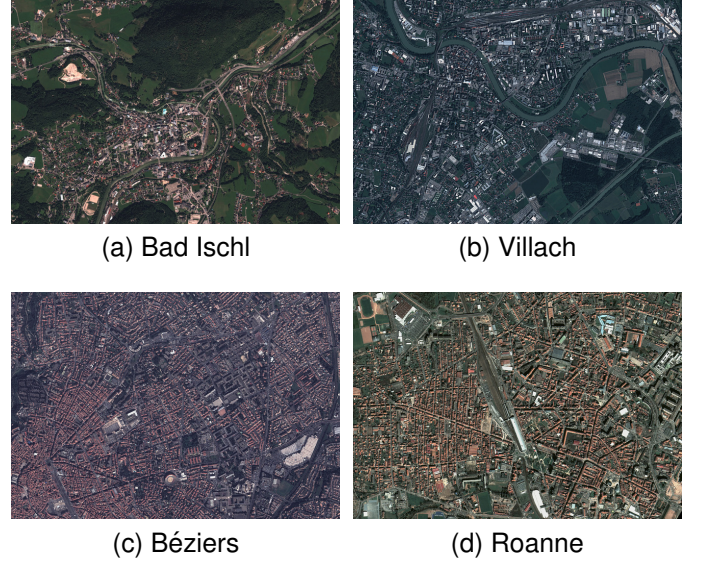


Fig. 5. Example close-ups from the Luxcarta dataset.

TABLE I
THE STATISTICS FOR THE LUXCARTA DATASET.

City	# of patches	Area (km ²)	Class frequency (%)		
			building	road	tree
<i>Bad Ischl</i>	84	27.71	5.51	6.03	35.38
<i>Villach</i>	138	43.59	9.26	10.63	19.91
<i>Béziers</i>	69	25.75	19.09	17.62	10.91
<i>Roanne</i>	60	25.84	18.44	8.33	14.78

between ColorMapGAN and CycleGAN, we replace the step 2 in our framework (see Fig. 2) with CycleGAN.

AdaptSegNet single [10]: Instead of generating fake images, this methodology aims to train a domain invariant network that can perform well in segmenting both training and test images. To do this, the classifier generates predicted maps from the training and the test images, and the discriminator forces the predicted maps for the test images to look like the predictions for the training images. In the original paper, DeepLab v2 [44] is used as the classifier. However, Atrous Spatial Pyramid Pooling (ASPP) in this network reduces the segmentation performance on satellite images significantly, especially when the image contains objects covering a small area. Hence, we remove ASPP from the network and upsample the final classification layer directly to get the predicted map with exactly the same size as the training images.

AdaptSegNet multiple [10]: In the same paper, in addition to aligning the final predictions for the training and test images, the experimental results with 2 classification layers and 2 discriminators are also presented. We compare our method with this strategy as well.

B. Experimental Setup

We use the Luxcarta dataset to conduct our experiments. The dataset contains 8 bit satellite images collected from 4 cities: *Bad Ischl* (Austria), *Villach* (Austria), *Béziers* (France), and *Roanne* (France). The spectral bands are red, green, blue, and the spatial resolution is 1m. The full annotations for

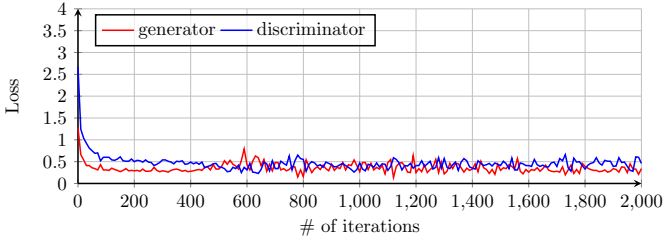


Fig. 6. # of iterations vs. loss plot when training ColorMapGAN to generate fake Béziers.

building, road, and tree classes are provided. An example close-up from each city is shown in Fig. 5. We split the cities into two pairs, where the first pair consists of *Bad Ischl* and *Villach*, and the second pair comprises *Béziers* and *Roanne*. To make the experimental setup suitable for the unsupervised domain adaptation problem, when we split the cities into pairs, we pay attention that radiometry of both cities in each pair is as different as possible, and that the objects belonging to the same class (e.g., building) have similar structural characteristics. For instance, buildings in *Béziers* and *Roanne* are densely grouped and have mostly rectangular shapes, whereas buildings in *Bad Ischl* and *Villach* are more sparsely distributed and mostly square-like shaped. However, as can be seen in Fig. 5, there is a large domain shift between spectral bands of the cities in each pair. Our final assumption is that we have an access to annotations of only the training city. For instance, when we classify *Roanne* in pair 2, we suppose that its annotations are not available; only the ground-truth of *Béziers* is accessible. Similarly, to classify *Béziers*, we assume that the ground-truth for only *Roanne* is accessible.

In the preprocessing step, we split each satellite image into 512×512 training patches with an overlap of 32 pixels between neighboring patches. Table I reports for each city the number of patches, the total area covered, and the class frequencies. For the quantitative performance assessment, we use Intersection over Union (IoU) [45] as the evaluation metric.

C. Training Details

In the first step of the end to end framework, we train a Unet with *Adam optimizer*, where the learning rate is 0.0001, exponential decay rate for the first and the second moment estimates are 0.9 and 0.999. In each iteration, we randomly sample a batch of 8 training patches. We apply online data augmentation with random horizontal/vertical flips and 0/90/180/270 degrees of rotations. We use sigmoid cross entropy as the loss function and ignore the background class while computing the loss. We optimize the network for 10,000 iterations.

In the stage of generating fake training images, in each training iteration of ColorMapGAN, we randomly sample only one patch from the training city and one patch from the test city. We use *Adam optimizer* to update both the generator and the discriminator. Since the generator is architecturally much simpler than the discriminator, we prefer to optimize it with a larger learning rate. For the generator, the learning rate

is 0.0005, whereas we set it to 0.0001 for the discriminator. Fig. 6 depicts the losses as the training iterations go on when generating fake *Béziers*. Because the losses for the other cities look almost the same, we prefer not to add them. We verify by visual inspection that visually appealing results are obtained at the 2,000th iteration. In addition, as can be seen from the plot that the losses seem to converge at that iteration. Therefore, we optimize ColorMapGAN for 2,000 iterations. We fine-tune the previously trained network on the fake training images for 3,000 iterations.

When we train CycleGAN, we use the default parameters specified in the original paper [24]. We use the default parameters for AdaptSegNet as well. For both of these methodologies, since 512×512 training patches do not fit to our GPU, we resize each patch to 256×256 before feeding it to the network.

D. Results

Fig. 7 illustrates some parts of the original training images from the pairs and the test stylized fake training images generated by the proposed ColorMapGAN and CycleGAN. From the fake training images generated by ColorMapGAN, we can see that colors of the test images are transferred to the fake training images successfully, while preserving the exact location of the objects. Moreover, the style of the test images are transferred to the fake training images successfully. CycleGAN also succeeds in transferring the colors to the fake training image, but spoils semantic identity of the training images. In Fig. 7, with green and yellow rectangles, we highlight some of the green and the residential areas that CycleGAN replaces by other semantically inconsistent artificial objects.

Fig. 9 illustrates histograms for color bands of the fake cities generated by ColorMapGAN and the original cities in pair 1. The number of pixels belonging to the same classes in *Villach* and *Bad Ischl* is not the same. Therefore, we cannot expect the color histogram of the original and the fake cities for each band to be exactly the same. However, we expect the histograms for the original as well the fake cities to resemble each other. The figure shows that the histograms of the cities in pair 1 are remarkably different. However, the histograms of *Villach* and fake *Bad Ischl*, and *Bad Ischl* and *Villach* are similar.

Tables II and III report IoU values for each method on the test cities. As expected, the performance of Unet without any adaptation is extremely low. As it can be confirmed by Fig. 8, when compared to Unet, visually much more appealing maps could be generated by the proposed end to end framework. Since the fake training images by CycleGAN and the original training images are semantically inconsistent, the fake images and the ground-truth do not match. Hence, utilizing the fake images generated by CycleGAN does not improve the results. The network architecture used in AdaptSegNet single is very deep; therefore, aligning only the outputs of the final classification layer for the training and the test images does not yield a good performance. However, if the alignment is performed in multiple layers, a better performance could be obtained, especially when the objects of interests cover a large area such as forests. For instance, *Bad Ischl* contains big forests; 35.38% of the pixels are labeled as tree as reported in Table I.

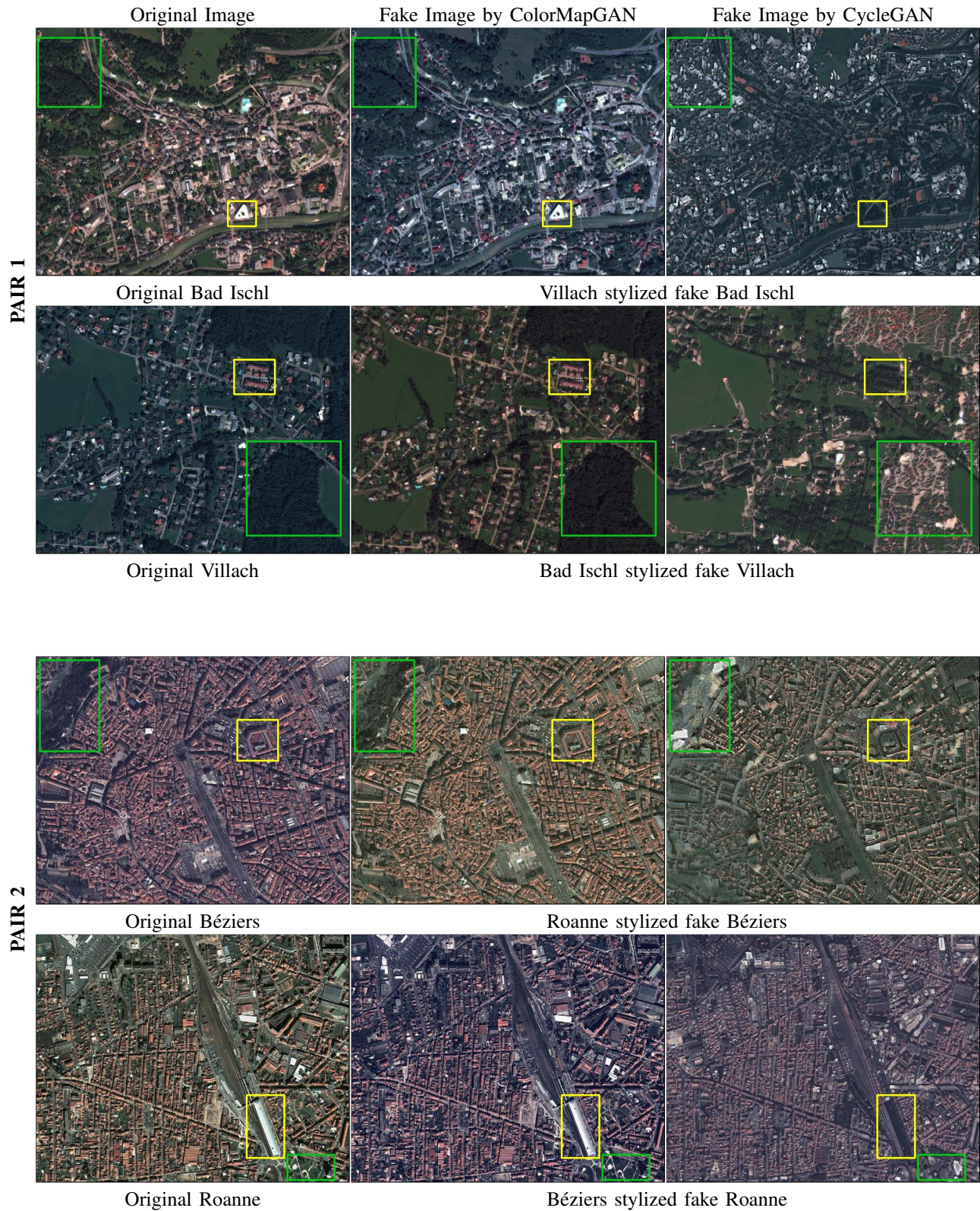


Fig. 7. The original images as well as the fake images generated by ColorMapGAN and CycleGAN. Left-column: some parts of the original training images from the city pairs, middle and right column: fake training images with the style of test images by ColorMapGAN (middle) and CycleGAN(right).

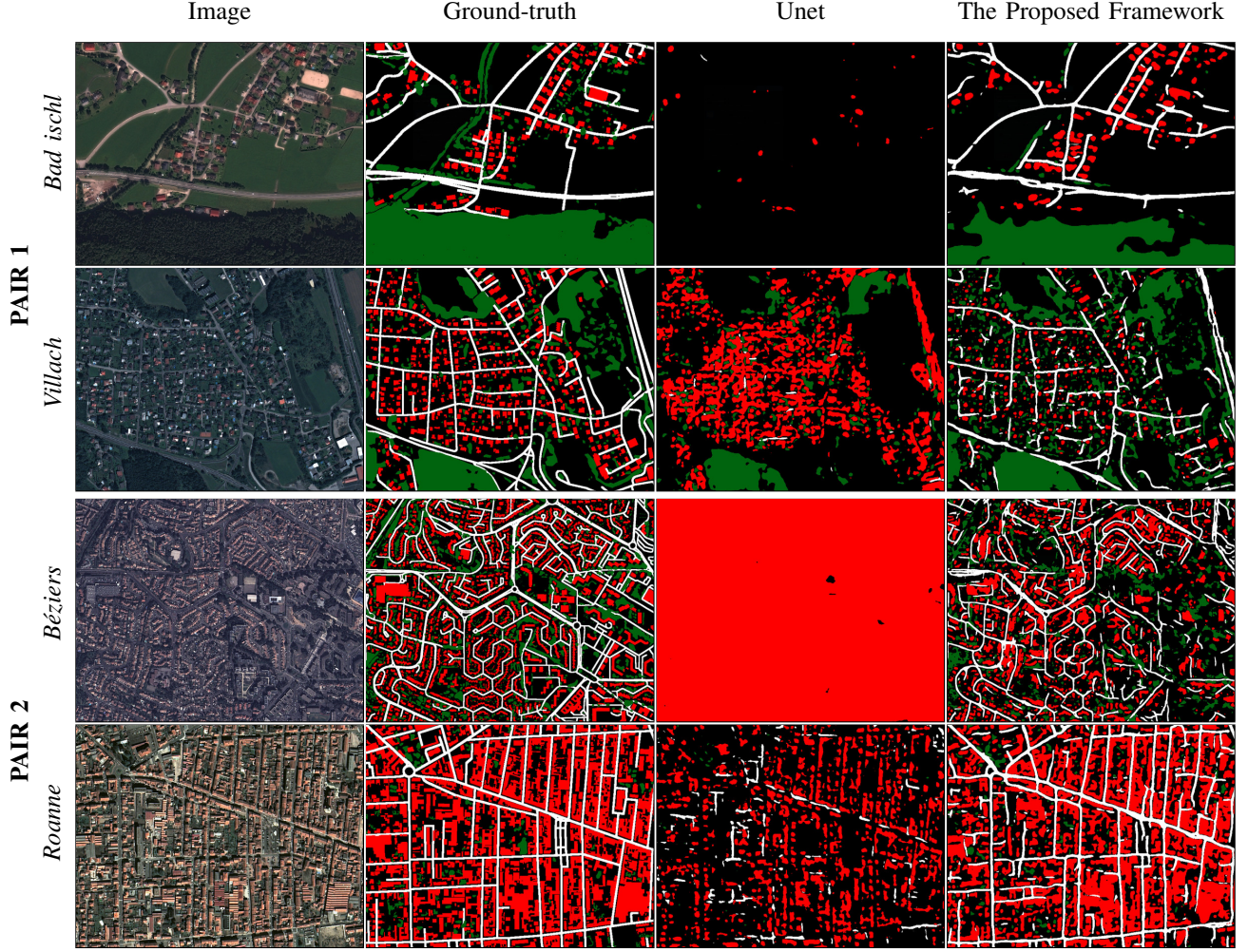


Fig. 8. Predictions by Unet and our framework. Building, road, and tree classes are represented by red, white, and green colors, respectively.

For tree class on this city, IoU value for AdaptSegNet multi is 60.57%, which is slightly lower than the performance of ColorMapGAN. However, the performance of AdaptSegNet is not satisfactory in segmenting small objects such as building and thin objects like roads. The tables demonstrate that the proposed end to end framework significantly outperforms the other approaches.

E. Running Times

The proposed framework and CycleGAN were implemented in Tensorflow¹. We conducted all the experiments on an Nvidia Geforce GTX1080 Ti GPU with 11 GB of RAM. Table IV reports the running times to train ColorMapGAN and CycleGAN for 1 iteration. The table demonstrates that although we feed 4 times larger training patches to ColorMapGAN than to CycleGAN, the training time of ColorMapGAN for each iteration is almost 7 times shorter. Let us also remark again that we optimize ColorMapGAN for only 2,000 iterations. In other words, we need only about 3 minutes and 20 seconds to train it. On the other hand, CycleGAN with the default parameters requires more than 3 hours to train.

¹<https://www.tensorflow.org>

V. CONCLUDING REMARKS

In this work, we presented a novel end to end framework to generate high quality maps from satellite images even when there exists a large domain shift between spectral bands of the training and the test images. We validated our approach on two city pairs, where we performed a city to city domain adaptation in each pair. Our experimental results demonstrated that the proposed framework exhibits a much better performance than the existing approaches. We also showed that the proposed ColorMapGAN generates fake images in a significantly shorter time than one of the competitive unpaired image to image translation methods in the computer vision community.

A possible future direction could be to investigate a more difficult domain adaptation problem, where in addition to the large spectral difference, shapes of the objects such as buildings in the training and test images are considerably different.

ACKNOWLEDGMENT

The authors would like to thank ACRI-ST and CNES for initializing and funding this study. The authors also thank Alain Giros and Sébastien Clerc for fruitful discussions.

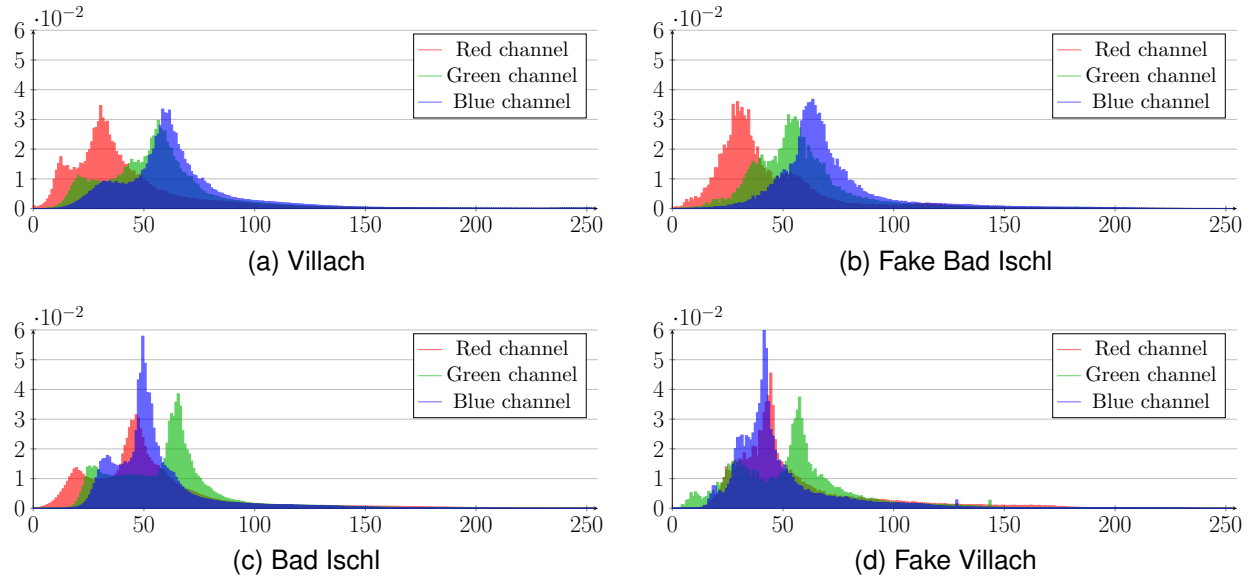


Fig. 9. The color histogram of the original cities and the fake cities generated by ColorMapGAN in pair 1. The histograms of Villach and Bad Ischl are largely different. The histograms of Villach \leftrightarrow fake Bad Ischl and Bad Ischl \leftrightarrow fake Villach resemble each other (best viewed in color).

TABLE II
IOU SCORES FOR THE TEST CITIES IN PAIR 1.

Method	Training: Bad Ischl, Test: Villach				Training: Villach, Test: Bad Ischl			
	building	road	tree	Overall	building	road	tree	Overall
<i>Unet</i>	23.61	0.91	40.53	21.68	5.84	0.24	0.50	2.19
<i>AdaptSegNet single</i>	0.00	1.45	22.69	8.05	2.65	2.29	1.51	2.15
<i>AdaptSegNet multi</i>	27.11	10.13	60.57	32.60	12.66	4.38	35.68	17.57
<i>The Proposed Framework with CycleGAN</i>	13.96	3.80	1.81	6.52	0.00	0.00	19.38	6.46
<i>The Proposed Framework</i>	26.73	24.57	61.43	37.58	44.48	37.75	42.75	41.66

TABLE III
IOU SCORES FOR THE TEST CITIES IN PAIR 2.

Method	Training: Béziers, Test: Roanne				Training: Roanne, Test: Béziers			
	building	road	tree	Overall	building	road	tree	Overall
<i>Unet</i>	26.13	11.16	7.79	15.03	19.85	0.00	0.00	6.62
<i>AdaptSegNet single</i>	0.80	9.62	1.38	3.93	18.18	5.09	0.73	8.00
<i>AdaptSegNet multi</i>	27.44	10.87	23.53	20.61	29.15	9.39	16.66	18.40
<i>The Proposed Framework with CycleGAN</i>	24.16	29.35	0.07	17.86	0.62	0.04	0.44	0.37
<i>The Proposed Framework</i>	52.19	41.92	32.80	40.30	32.16	32.48	19.78	28.14

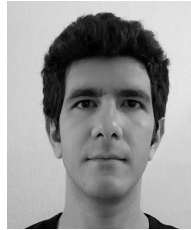
TABLE IV
TRAINING TIMES FOR GENERATING FAKE CITIES IN PAIR 1.

Method	Patch Size	Training Time for 1 Iter. (seconds)
ColorMapGAN	512×512	0.1
CycleGAN	256×256	0.67

REFERENCES

- [1] O. Ronneberger, P. Fischer, and T. Brox, “U-net: Convolutional networks for biomedical image segmentation,” in *MICCAI*. Springer, 2015, pp. 234–241.
- [2] V. Iglovikov and A. Shvets, “Ternausnet: U-net with vgg11 encoder pre-trained on imagenet for image segmentation,” *arXiv*, 2018.
- [3] V. Iglovikov, S. Seferbekov, A. Buslaev, M. R. Center, and A. Shvets, “Ternausnetv2: Fully convolutional network for instance segmentation,” *arXiv*, 2018.
- [4] E. Maggiori, Y. Tarabalka, G. Charpiat, and P. Alliez, “High-resolution aerial image labeling with convolutional neural networks,” *IEEE TGRS*, vol. 55, no. 12, pp. 7092–7103, 2017.
- [5] B. Huang, K. Lu, N. Audebert, A. Khalef, Y. Tarabalka, J. Malof, A. Boulch, B. Le Saux, L. Collins, K. Bradbury *et al.*, “Large-scale semantic classification: outcome of the first year of inria aerial image labeling benchmark,” in *IEEE IGARSS*, 2018.
- [6] O. Tasar, Y. Tarabalka, and P. Alliez, “Incremental learning for semantic segmentation of large-scale remote sensing data,” *arXiv*, 2018.
- [7] J. Hoffman, D. Wang, F. Yu, and T. Darrell, “Fcns in the wild: Pixel-level adversarial and constraint-based adaptation,” *arXiv*, 2016.
- [8] S. Sankaranarayanan, Y. Balaji, A. Jain, S. Nam Lim, and R. Chellappa, “Learning from synthetic data: Addressing domain shift for semantic segmentation,” in *IEEE CVPR*, 2018, pp. 3752–3761.
- [9] Z. Murez, S. Kolouri, D. Kriegman, R. Ramamoorthi, and K. Kim, “Image to image translation for domain adaptation,” in *IEEE CVPR*, 2018, pp. 4500–4509.
- [10] Y.-H. Tsai, W.-C. Hung, S. Schuster, K. Sohn, M.-H. Yang, and M. Chandraker, “Learning to adapt structured output space for semantic segmentation,” in *IEEE CVPR*, 2018, pp. 7472–7481.
- [11] H. Huang, Q. Huang, and P. Krahenbuhl, “Domain transfer through deep activation matching,” in *ECCV*, 2018, pp. 590–605.
- [12] W. Hong, Z. Wang, M. Yang, and J. Yuan, “Conditional generative adversarial network for structured domain adaptation,” in *IEEE CVPR*, 2018, pp. 1335–1344.
- [13] K. Saito, K. Watanabe, Y. Ushiku, and T. Harada, “Maximum classifier discrepancy for unsupervised domain adaptation,” in *IEEE CVPR*, 2018, pp. 3723–3732.

- [14] Y. Zhang, P. David, and B. Gong, "Curriculum domain adaptation for semantic segmentation of urban scenes," in *IEEE ICCV*, 2017, pp. 2020–2030.
- [15] Y. Chen, W. Li, and L. Van Gool, "Road: Reality oriented adaptation for semantic segmentation of urban scenes," in *IEEE CVPR*, 2018, pp. 7892–7901.
- [16] O. Russakovsky, J. Deng, H. Su, J. Krause, S. Satheesh, S. Ma, Z. Huang, A. Karpathy, A. Khosla, M. Bernstein *et al.*, "Imagenet large scale visual recognition challenge," *IJCV*, vol. 115, no. 3, pp. 211–252, 2015.
- [17] J. Zhang, C. Liang, and C.-C. J. Kuo, "A fully convolutional tri-branch network (fctn) for domain adaptation," in *IEEE ICASSP*. IEEE, 2018, pp. 3001–3005.
- [18] Y. Zou, Z. Yu, B. Vijaya Kumar, and J. Wang, "Unsupervised domain adaptation for semantic segmentation via class-balanced self-training," in *ECCV*, 2018, pp. 289–305.
- [19] R. Romijnders, P. Meletis, and G. Dubbelman, "A domain agnostic normalization layer for unsupervised adversarial domain adaptation," *arXiv*, 2018.
- [20] K. Saito, Y. Ushiku, T. Harada, and K. Saenko, "Adversarial dropout regularization," *arXiv*, 2017.
- [21] X. Pan, P. Luo, J. Shi, and X. Tang, "Two at once: Enhancing learning and generalization capacities via ibn-net," in *ECCV*, 2018, pp. 464–479.
- [22] X. Zhu, H. Zhou, C. Yang, J. Shi, and D. Lin, "Penalizing top performers: Conservative loss for semantic segmentation adaptation," in *ECCV*, 2018, pp. 568–583.
- [23] D. Ulyanov, A. Vedaldi, and V. Lempitsky, "Instance normalization: The missing ingredient for fast stylization," *arXiv*, 2016.
- [24] J.-Y. Zhu, T. Park, P. Isola, and A. A. Efros, "Unpaired image-to-image translation using cycle-consistent adversarial networks," in *IEEE CVPR*, 2017, pp. 2223–2232.
- [25] M.-Y. Liu, T. Breuel, and J. Kautz, "Unsupervised image-to-image translation networks," in *NIPS*, 2017, pp. 700–708.
- [26] X. Huang, M.-Y. Liu, S. Belongie, and J. Kautz, "Multimodal unsupervised image-to-image translation," in *ECCV*, 2018, pp. 172–189.
- [27] H.-Y. Lee, H.-Y. Tseng, J.-B. Huang, M. Singh, and M.-H. Yang, "Diverse image-to-image translation via disentangled representations," in *ECCV*, 2018, pp. 35–51.
- [28] J. Hoffman, E. Tzeng, T. Park, J.-Y. Zhu, P. Isola, K. Saenko, A. A. Efros, and T. Darrell, "Cycada: Cycle-consistent adversarial domain adaptation," *arXiv*, 2017.
- [29] L. A. Gatys, A. S. Ecker, and M. Bethge, "Image style transfer using convolutional neural networks," in *IEEE CVPR*, 2016, pp. 2414–2423.
- [30] L. A. Gatys, M. Bethge, A. Hertzmann, and E. Shechtman, "Preserving color in neural artistic style transfer," *arXiv*, 2016.
- [31] J. Johnson, A. Alahi, and L. Fei-Fei, "Perceptual losses for real-time style transfer and super-resolution," in *ECCV*. Springer, 2016, pp. 694–711.
- [32] D. Ulyanov, V. Lebedev, A. Vedaldi, and V. S. Lempitsky, "Texture networks: Feed-forward synthesis of textures and stylized images," in *ICML*, vol. 1, no. 2, 2016, p. 4.
- [33] S. J. Pan, I. W. Tsang, J. T. Kwok, and Q. Yang, "Domain adaptation via transfer component analysis," *IEEE Transactions on Neural Networks*, vol. 22, no. 2, pp. 199–210, 2011.
- [34] G. Matasci, M. Volpi, M. Kanevski, L. Bruzzone, and D. Tuia, "Semisupervised transfer component analysis for domain adaptation in remote sensing image classification," *IEEE TGRS*, vol. 53, no. 7, pp. 3550–3564, 2015.
- [35] Y. Qin, L. Bruzzone, B. Li, and Y. Ye, "Tensor alignment based domain adaptation for hyperspectral image classification," *arXiv*, 2018.
- [36] P. Isola, J.-Y. Zhu, T. Zhou, and A. A. Efros, "Image-to-image translation with conditional adversarial networks," in *IEEE CVPR*, 2017, pp. 1125–1134.
- [37] I. Goodfellow, J. Pouget-Abadie, M. Mirza, B. Xu, D. Warde-Farley, S. Ozair, A. Courville, and Y. Bengio, "Generative adversarial nets," in *NIPS*, 2014, pp. 2672–2680.
- [38] A. Radford, L. Metz, and S. Chintala, "Unsupervised representation learning with deep convolutional generative adversarial networks," *arXiv*, 2015.
- [39] M. Arjovsky, S. Chintala, and L. Bottou, "Wasserstein gan," *arXiv*, 2017.
- [40] I. Gulrajani, F. Ahmed, M. Arjovsky, V. Dumoulin, and A. C. Courville, "Improved training of wasserstein gans," in *NIPS*, 2017, pp. 5767–5777.
- [41] X. Mao, Q. Li, H. Xie, R. Y. Lau, Z. Wang, and S. Paul Smolley, "Least squares generative adversarial networks," in *IEEE ICCV*, 2017, pp. 2794–2802.
- [42] M. Mirza and S. Osindero, "Conditional generative adversarial nets," *arXiv*, 2014.
- [43] B. Xu, N. Wang, T. Chen, and M. Li, "Empirical evaluation of rectified activations in convolutional network," *arXiv*, 2015.
- [44] L.-C. Chen, G. Papandreou, I. Kokkinos, K. Murphy, and A. L. Yuille, "DeepLab: Semantic image segmentation with deep convolutional nets, atrous convolution, and fully connected crfs," *IEEE TPAMI*, vol. 40, no. 4, pp. 834–848, 2018.
- [45] G. Csarka, D. Larlus, F. Perronnin, and F. Meylan, "What is a good evaluation measure for semantic segmentation?," in *BMVC*, vol. 27. Citeseer, 2013, p. 2013.



Onur Tasar received the B.S. degree in computer engineering department from Hacettepe University, Ankara, Turkey in 2014, and the M.S. degree in computer engineering department from Bilkent University, Ankara, Turkey in 2017. He is currently working towards his Ph.D. at Inria Sophia Antipolis-Méditerranée within TITANE team, Valbonne, France.

His research interests include computer vision, machine learning, and computational geometry with applications to remote sensing.



S L Happy He has completed the joint MS – PhD degree from Indian Institute of Technology Kharagpur, India in 2018. Currently, he is working as a postdoctoral researcher in Inria Sophia Antipolis, France. His research interests include machine learning, computer vision, hyperspectral image classification, medical image analysis, and facial expression analysis.



Yuliya Tarabalka (S'08–M'10) received the B.S. degree in computer science from Ternopil Ivan Pul'uj State Technical University, Ukraine, in 2005 and the M.Sc. degree in signal and image processing from the Grenoble Institute of Technology (INPG), France, in 2007. She received a joint Ph.D. degree in signal and image processing from INPG and in electrical engineering from the University of Iceland, in 2010.

From July 2007 to January 2008, she was a researcher with the Norwegian Defence Research Establishment, Norway. From September 2010 to December 2011, she was a postdoctoral research fellow with the Computational and Information Sciences and Technology Office, NASA Goddard Space Flight Center, Greenbelt, MD. From January to August 2012 she was a postdoctoral research fellow with the French Space Agency (CNES) and Inria Sophia Antipolis-Méditerranée, France. From 2012 to 2019 she was a researcher with the TITANE team of Inria Sophia Antipolis-Méditerranée. She is currently the research director of LuxCarta Technology. Her research interests are in the areas of image processing, pattern recognition and development of efficient algorithms. She is Member of the IEEE Society.



Pierre Alliez Pierre Alliez is Senior Researcher and team leader at Inria Sophia-Antipolis - Méditerranée. He has authored scientific publications and several book chapters on mesh compression, surface reconstruction, mesh generation, surface remeshing and mesh parameterization. He was awarded in 2005 the EUROGRAPHICS young researcher award for his contributions to computer graphics and geometry processing. He was co-chair of the Symposium on Geometry Processing in 2008, of Pacific Graphics in 2010 and Geometric Modeling and Processing

2014. He was awarded in 2011 a Starting Grant from the European Research Council on Robust Geometry Processing. He is an associate editor of the ACM Transactions on Graphics.